Copy
RM L56G24

X80K-04

NACA RM L56G24

NACA

RESEARCH MEMORANDUM

SUPERSONIC INVESTIGATION OF THE LIFT, DRAG, STATIC STABILITY, AND HINGE-MOMENT CHARACTERISTICS OF A ROCKET-POWERED MODEL OF A BALLISTIC-MISSILE CONFIGURATION

By Warren Gillespie, Jr.

Langley Aeronautical Laboratory
Langley Field, Va.

NATIONAL ADVISORY COMMITTEE FOR AERONAUTICS

WASHINGTON

September 28, 1956

NATIONAL ADVISORY COMMITTEE FOR AERONAUTICS

RESEARCH MEMORANDUM

SUPERSONIC INVESTIGATION OF THE LIFT, DRAG, STATIC STABILITY, AND HINGE-MOMENT CHARACTERISTICS OF A ROCKET-POWERED MODEL OF A BALLISTIC-MISSILE CONFIGURATION

By Warren Gillespie, Jr.

SUMMARY

A free-flight investigation was made to determine the lift, drag, static stability, and hinge-moment characteristics of a rocket-powered model of a ballistic-missile configuration at supersonic speeds. The model consisted essentially of a body of fineness ratio 16.9 and a cruciform set of small 60° delta fins located approximately 1 body diameter from the base of the body. The model was aerodynamically pulsed (in pitch) by two of the fins. Drag polars, normal-force and hinge-moment coefficients, and static stability were determined over a Mach number range of 1.6 to 2.1. Axial-drag and side-force coefficients were obtained over a Mach number range of 1.6 to 2.8.

The model lift and pitching-moment coefficients were nonlinear with angle of attack. The method of NACA Research Memorandum L52D22 satisfactorily estimated the components of lift at zero angle of attack. Static stability increased with angle of attack and normal-force coefficient but decreased at zero angle of attack with increasing Mach number, and was indicated to be zero at a Mach number of approximately 3.1 for a center-of-gravity location at 0.46 body length. The fin aerodynamic center was at 0.49 mean aerodynamic chord of the exposed fin. The model experienced combined pitch, yaw, and roll motions and crossed the stability boundary associated with a rolling missile.

INTRODUCTION

The ballistic rocket-propelled missile, while inherently a simple aerodynamic configuration, poses a complex stability and control problem because of the great variation in flight conditions engendered by the

requirement that the missile have a sufficient range capability. Two or more stabilization and control systems in one missile are frequently used to insure successful flight in a rapidly changing environment. However, if the acceleration at take-off is sufficiently high and the trajectory is entirely within the atmosphere (dynamic pressure $\gtrsim$ 10 lb/sq ft), the use of aerodynamic fins alone may be satisfactory, depending on the degree of aerodynamic heating and the matching of aerodynamic-center and center-of-gravity variations with Mach number and flight time, respectively.

The purpose of the present investigation was to determine the lift, drag, static stability, and hinge-moment characteristics of a missile configuration having a long run of boundary layer ahead of small 60° delta stabilizing fins. The model was flight tested over a range of Mach number from 1.6 to 2.8 at the Langley Pilotless Aircraft Research Station at Wallops Island, Va. After separation from the booster, the model was pulsed (in pitch) by two of the fins, and the basic aerodynamic parameters were determined from the response of the model to the tail deflections.

SYMBOLS

C_N normal-force coefficient, $\frac{a_n}{g}\frac{W/S_B}{q}$

C_Y side-force coefficient, $\frac{a_y}{g}\frac{W/S_B}{q}$

C_X axial-force coefficient, $\frac{a_x}{g}\frac{W/S_B}{q}$

C_R resultant transverse-force coefficient, $\sqrt{C_N^2 + C_Y^2}$

C_L lift coefficient, $C_R \cos \alpha_R + C_X \sin \alpha_R$

C_D drag coefficient, $-C_X \cos \alpha_R + C_R \sin \alpha_R$

C_m pitching-moment coefficient about the center of gravity, $\frac{I_Y \ddot{\theta}}{qS_B d}$

C_h fin hinge-moment coefficient, $\frac{H}{qS_F \bar{c}}$

$C_{N_\alpha} = \left(\frac{\partial C_N}{\partial \alpha}\right)_{C_N=0}$

$$C_{N_\delta} = \left(\frac{\partial C_N}{\partial \delta}\right)_{C_N=0}$$

$$C_{Y_\beta} = \left(\frac{\partial C_Y}{\partial \beta}\right)_{C_Y=0}$$

$$C_{h_{\alpha_F}} = \left(\frac{\partial C_h}{\partial \alpha_F}\right)_{C_h=0}$$

a_n, a_y, a_x normal, lateral, and axial accelerations, respectively, ft/sec^2

g acceleration due to gravity, 32.2 ft/sec^2

q dynamic pressure, lb/sq ft

H hinge moment of one fin about its hinge line, ft-lb

M Mach number

W weight of model, 177.2 lb during first coast period and 131.0 lb during second coast

α angle of attack at model center of gravity, deg

α_F angle of attack at fin, deg

β angle of sideslip at model center of gravity, deg

α_R resultant angle of inclination, $\sqrt{\alpha^2 + \beta^2}$, deg

$\dot{\phi}$ rolling velocity, radians/sec

$\ddot{\theta}$ angular acceleration in pitch, radians/sec^2

δ horizontal fin deflection from body center line, deg

I_Y model moment of inertia in pitch about center of gravity, 50.0 slug-ft^2 during first coast period and 44.2 slug-ft^2 during second coast

S_B body maximum circular cross-sectional area, 0.27 sq ft

S_F exposed area of one horizontal fin, 0.18 sq ft

d body maximum diameter, 0.58 ft

$\bar{c}$ exposed mean aerodynamic chord of a horizontal fin, 0.52 ft

X, Y, Z missile body axes (see fig. 1)

MODEL

A drawing of the model is shown in figure 2 and photographs of the model are presented in figures 3, 4, and 5. Contour ordinates of the nose are listed in table I. The configuration had a body of revolution of fineness ratio 16.9 and four small 60° delta tail fins mounted in a cruciform arrangement on the body at approximately 1 body diameter from the base of the body. The ratio of the maximum diameter of the body to the tail span was 0.433. The fin airfoil section was a beveled flat plate of 4-percent maximum thickness. The trailing edge of the vertical fins was extended 0.47 inch rearward to accommodate the telemeter antenna.

The two horizontal fins were free to rotate about separate hinge lines. The hinge line for the left fin was located at 0.65 of the exposed mean aerodynamic chord and the right fin at 0.55. The two fins were statically balanced about their respective hinge lines and free to rotate between stop settings of approximately 2.4° and -1.7°. To insure that the two separately hinged fins would move off the stops approximately in unison, a crossover yoke was used which permitted 0.5° relative movement between the two fins. The yoke did not interfere with the measurement of the separate hinge moments during the time the fins were against the stops. Each stop was an integral part of a cantilever-beam system used to measure the fin hinge moments. The stiffness of the individual hinge-moment beams was designed to give approximately equal additional fin deflections for the maximum hinge moments expected during the flight test.

The model was of metal construction. A sustainer rocket motor was carried inside the fuselage in addition to a telemeter with angle-of-attack, angle-of-sideslip, pressure, hinge-moment, and accelerometer instruments. Because of the presence of the rocket motor the accelerometer instruments near the model center of gravity protruded somewhat beyond the 7-inch body diameter. Fairings were used to enclose these instruments. The model was externally boosted by the simultaneous firing of the two Deacon rockets shown in figure 5.

TEST

Some hinge-moment data were obtained during boosted flight. However, most of the data were obtained during ascent of the model after separation from the booster. The model was then pulsed in pitch by the horizontal tail fins each time the lift on the fins reversed direction. A more complete description of this technique is given in reference 1.

The quantities measured by the telemeter system were normal, longitudinal, and lateral accelerations; angles of attack and sideslip; hinge moments; and total pressure. Total pitching moment was measured by the difference in reading of two normal accelerometers located a distance apart. The velocity obtained from a CW Doppler radar set (corrected for wind velocity) was used in conjunction with tracking radar and radiosonde data to calculate Mach number, Reynolds number, and dynamic pressure. Ground rollsonde equipment operating with the directional telemeter antenna signal from the model indicated the model rolling velocity. The variation of the free-stream Reynolds number per foot of length and dynamic pressure with Mach number is shown in figure 6(a). There was a coasting period before and after the period of flight with sustainer power on. The ranges of the maximum angles of attack, induced sideslip angles, and rolling velocities are shown in figure 6(b). The method of data reduction was similar to that used in reference 2.

ACCURACY AND CORRECTIONS

The Mach number is estimated to be accurate to ±1 percent. Errors in aerodynamic coefficients can arise because of dynamic-pressure inaccuracies, which are approximately twice as large as the error in Mach number. Thus all coefficients have a probable error of at least ±2 percent. The maximum absolute accuracy of a telemetered quantity obtained from a single instrument is usually better than 2 percent of the total calibrated instrument range. The probable error is approximately 1 percent. Reference 3 indicates the accuracy that can be expected of a typical flow indicator working without the telemeter apparatus. An additional source of inaccuracy in the final results may be the induced sideslip and rolling motions.

Measurements obtained from the flow indicator were corrected for pitching and yawing velocities and for flight-path curvature. Position corrections were made to measurements obtained from the normal, lateral, and longitudinal accelerometers mounted near the center of gravity of the model.

The probable errors are estimated to be less than the following possible limits of accuracy:

α, deg	±0.4
β, deg	±0.4
C_N	±0.04
C_Y	±0.04
C_X	±0.015
C_m	±0.2
C_h	±0.003

RESULTS AND DISCUSSION

General

Most of the data were obtained during the first coast period. Shortly after the sustainer motor fired, large-amplitude oscillations occurred in rolling velocity. Estimates based on the charts of reference 4 indicated that the stability boundary for the rolling model was crossed. The variation of the angles of attack and sideslip became irregular and the pulsing of the tail fins was erratic. After burnout of the rocket motor, the model rolled steadily at 22 to 15 radians per second and the angles of attack and sideslip reduced to near-zero values. The fins stopped pulsing with the left fin at approximately 2.4° setting and the right fin apparently hung up against the crossover yoke. By using figure 7 it is possible to explain the excessive model rolling. The deflections of the left and right fins became slightly different from each other as the angle of attack increased in absolute magnitude. The model therefore received small pulses in roll as well as pulses in pitch. However, it is also possible that a similar pattern of motion might have occurred even with identical deflections of the left and right fins, since it is known that rolling moments due to combined angles of attack and sideslip and aerodynamic asymmetry of the tail deflection would still exist.

Drag

The axial drag-coefficient data obtained independently from a high-range accelerometer and from one having a lower range are presented in figure 8 as a function of Mach number for angles of attack near zero and absolute values of sideslip angle approximately equal to or less than ±7°. The values from the two accelerometers are in excellent agreement. Data points between Mach numbers of 2.11 and 2.55 (obtained during the second

coast period) are not presented. These data were unexplainably higher by approximately an increment of 0.03. The data show that the coefficient $-C_X$ decreased linearly with an increase in Mach number. The dashed curve was obtained by extrapolation of the drag polars presented in figure 9 for the additional condition of zero sideslip angle. This curve is slightly lower than the axial drag curve obtained for the model at small angles of sideslip.

Figure 9 shows that the axial drag coefficient increased approximately linearly with the resultant transverse-force coefficient C_R for constant values of supersonic Mach number. At higher values of C_R (beyond the test range) a decrease in axial drag coefficient would be expected, since for an angle of inclination of 90° the axial drag coefficient for the model must be close to zero. A comparison of the drag of the finless model of reference 2 with the total drag determined for the present test model indicates that the body contributes approximately 75 percent of the total drag at a Mach number of 1.76.

The variation of the drag-due-to-lift parameter $\Delta C_D/C_L{}^2$ with resultant angle of attack (not presented) was similar to that shown in figures 8(b) and 11(b) of reference 5 for the body and body-fin models, respectively, of that investigation. That is, the parameter $\Delta C_D/C_L{}^2$ decreased slightly with increasing angle of attack. This decrease is probably caused by an increase in lift effectiveness of the body with increasing angle of attack.

Force Characteristics

Figures 10, 11, and 12 present the normal-force, side-force, and force-curve-slope parameters, respectively. In figure 10 the correction necessary to convert measured C_N values to values of C_N corresponding to constant tail settings of 2.41° and -1.70° (see fig. 7) is shown to be negligible for a Mach number of 2.08. Therefore the data points at the other Mach numbers of 2.01, 1.90, 1.76, and 1.71 were not similarly corrected. The variation of the normal and side-force coefficients with angle of inclination is nonlinear. The force-curve slopes C_{N_α} and $-C_{Y_\beta}$ increase with α and β, respectively.

Figure 12 shows that values of C_{N_α} and $-C_{Y_\beta}$ determined at zero angle of inclination are approximately of equal magnitude. From this comparison it appears that the accelerometer instrument fairings located on the top and bottom of the body were not significantly effective in producing additional side force. The force-curve slopes C_{N_α} and $-C_{Y_\beta}$ are in good agreement with the theoretical estimates made by the method of

reference 6. For Mach numbers greater than approximately 2.1, the experimental curve rises several percent above the theoretical. The lift effectiveness of the tail is also presented in figure 12. By using the method of reference 6, the variation with Mach number of the lift on the exposed tail panels due to angle of attack $\left(C_{N_\alpha}\right)_{\text{tail panel loading}}$ and due to tail deflection $\left(C_{N_\delta}\right)_{\text{tail panel loading}}$ was calculated, and a comparison is made with the experimental results obtained indirectly from the hinge-moment determinations of C_{h_α} and $\left(\frac{\Delta C_h}{\Delta \delta}\right)_{\alpha=0}$. The agreement is good. However, values of $\Delta C_N/\Delta\delta$ obtained from the curves of figures 10 and 13 appear to be too low, since the tail lift contribution determined in this manner includes the additional lift on the body due to tail deflection. This discrepancy may be partly due to the inaccuracy of the data indicated by the scatter of the slope values plotted in figure 12.

Pitching Moment and Static Stability

The pitching-moment characteristics of the model are presented in figures 13 and 14. An adjustment was made to the data corresponding to a Mach number of 2.08 to account for the effect on C_m of the small increase with angle of attack of the tail deflection (shown in fig. 7). Since the correction was found to be negligible, the data for Mach numbers of 2.01, 1.90, 1.76, and 1.71 were not similarly adjusted. A nonlinear variation of the pitching-moment coefficient with both angle of attack and normal-force coefficient is evident. Figures 13 and 14 indicate that the static stability of the model increases with increased angle of attack and normal-force coefficient. Figure 15 further shows that for zero angle of attack the aerodynamic center moved forward rapidly with an increase in Mach number. Calculations based on the method of reference 6 were in good agreement with the experimental values. The static stability is indicated to be zero at a Mach number of approximately 3.1 for a center-of-gravity location at 0.46 body length (station 54.4).

Hinge-Moment Characteristics

Figure 16 shows the hinge-moment data obtained from separate measurements of the left and right fins which were hinged at $0.65\bar{c}$ and $0.55\bar{c}$ (exposed), respectively. The measurements for the right fin at a deflection of -1.70° were in error and are not presented. The coefficients are plotted against values of angle of attack which were corrected for position error back to the fin location on the body rather than to the center-of-gravity location of the model. The variation of the measured hinge-moment coefficients with angle of attack is approximately linear but

includes some effect of tail-setting variation with angle of attack (fig. 7) and some effect of rolling. The basic data of figure 16 were used in the preparation of figures 17 and 18. In the determination of the hinge-moment parameter $C_{h_{\alpha_F}}$ the variation of the tail deflection with angle of attack was taken into account. Values of $\Delta C_h/\Delta\delta$ were obtained from hinge moments measured during boost of the model at zero angle of attack. The parameters $C_{h_{\alpha_F}}$ and $\Delta C_h/\Delta\delta$ generally decrease with increasing Mach number. A comparison is made at a Mach number of 1.72 with hinge-moment data reported in reference 7 for the Hermes missile configuration which also had small 60° delta stabilizing fins mounted at the end of a relatively shorter body than the present test configuration. The Hermes values adjusted to hinge lines of $0.65\bar{c}$ and $0.55\bar{c}$ are lower, in general, than the present-test values. Figure 18 shows that the fin aerodynamic center corresponding either to angle-of-attack loading or tail-deflection loading is at approximately $0.49\bar{c}$, and in good agreement with the results of reference 7.

SUMMARY OF RESULTS

Results obtained from a flight test of a finned ballistic-missile configuration at supersonic speeds lead to the following observations.

1. Lift and pitching-moment coefficients were nonlinear with angle of attack. The method of NACA Research Memorandum L52D22 satisfactorily estimated the components of lift of the body-tail configuration at zero angle of attack.

2. Static stability increased with angle of attack and lift but decreased at zero angle of attack with increasing Mach number. At a Mach number of approximately 3.1, for a center-of-gravity location at 0.46 body length, the static stability at zero angle of attack was indicated to be zero.

3. The fin aerodynamic-center location was at 0.49 mean aerodynamic chord of the exposed fin.

4. The model in experiencing combined pitch, yaw, and roll motions crossed the stability boundary associated with a rolling missile.

Langley Aeronautical Laboratory,
National Advisory Committee for Aeronautics,
Langley Field, Va., July 11, 1956.

REFERENCES

1. Gillespie, Warren, Jr., and Dietz, Albert E.: Use of an Aerodynamically Pulsed All-Movable Horizontal Tail to Obtain Longitudinal Characteristics of Rocket-Powered Models in Free Flight and Some Initial Results From an Arrow-Wing-Body-Tail Configuration. NACA RM L52C10, 1952.

2. Gillespie, Warren, Jr.: Free-Flight Determination of Force and Stability Characteristics of an Inclined Body of Fineness Ratio 16.9 at a Mach Number of 1.74. NACA RM L54G28a, 1954.

3. Ikard, Wallace L.: An Air-Flow-Direction Pickup Suitable for Telemetering Use on Pilotless Aircraft. NACA RM L53K16, 1954.

4. Bergrun, Norman R., and Nickel, Paul A.: A Flight Investigation of the Effect of Steady Rolling on the Natural Frequencies of a Body-Tail Combination. NACA TN 2985, 1953.

5. Spahr, J. Richard: Longitudinal Aerodynamic Characteristics to Large Angles of Attack of a Cruciform Missile Configuration at a Mach Number of 2. NACA RM A54H27, 1954.

6. Tucker, Warren A.: A Method for Estimating the Components of Lift of Wing-Body Combinations at Supersonic Speeds. NACA RM L52D22, 1952.

7. Thomas, Nancy: Hermes Configuration N_7T_{15}, Wind Tunnel Tests of Normal Force, Drag, and Elevator Effectiveness at M = 1.72. Rep. R51A0510, U. S. Army Ord. Project Hermes, Gen. Elec. Co., Jan. 1951.

TABLE I.- CONTOUR ORDINATES OF NOSE

Station, in. from nose	Body radius, in.
0	0.17
.06	.18
.12	.21
.24	.22
.48	.28
.73	.35
1.22	.46
2.00	.64
2.45	.73
4.80	1.24
7.35	1.72
8.00	1.85
9.80	2.15
12.25	2.50
13.12	2.61
14.37	2.75
14.70	2.78
17.15	3.01
19.60	3.22
22.05	3.38
24.50	3.50
25.00	3.50

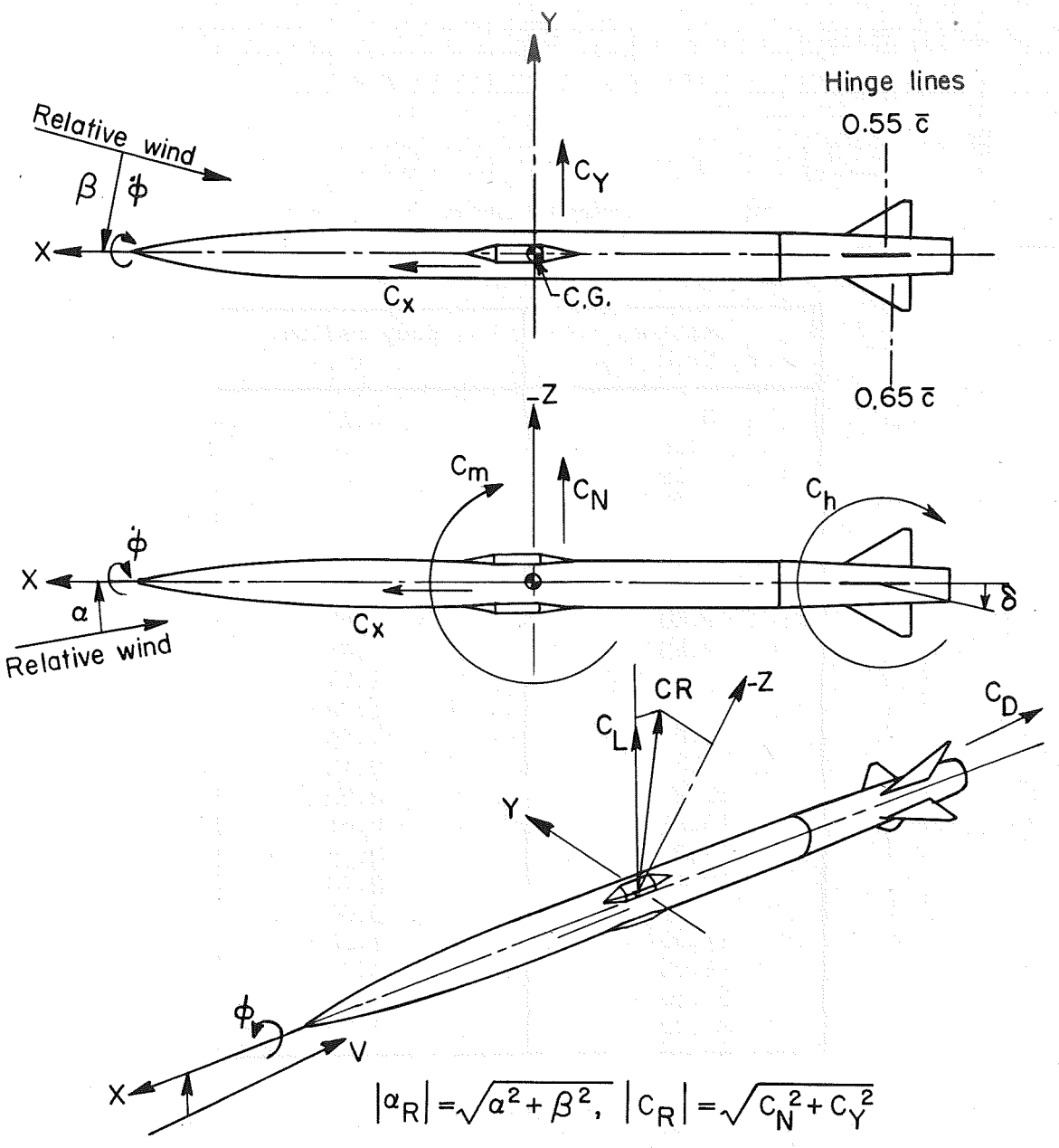

Figure 1.- System of axes. Arrows indicate positive directions.

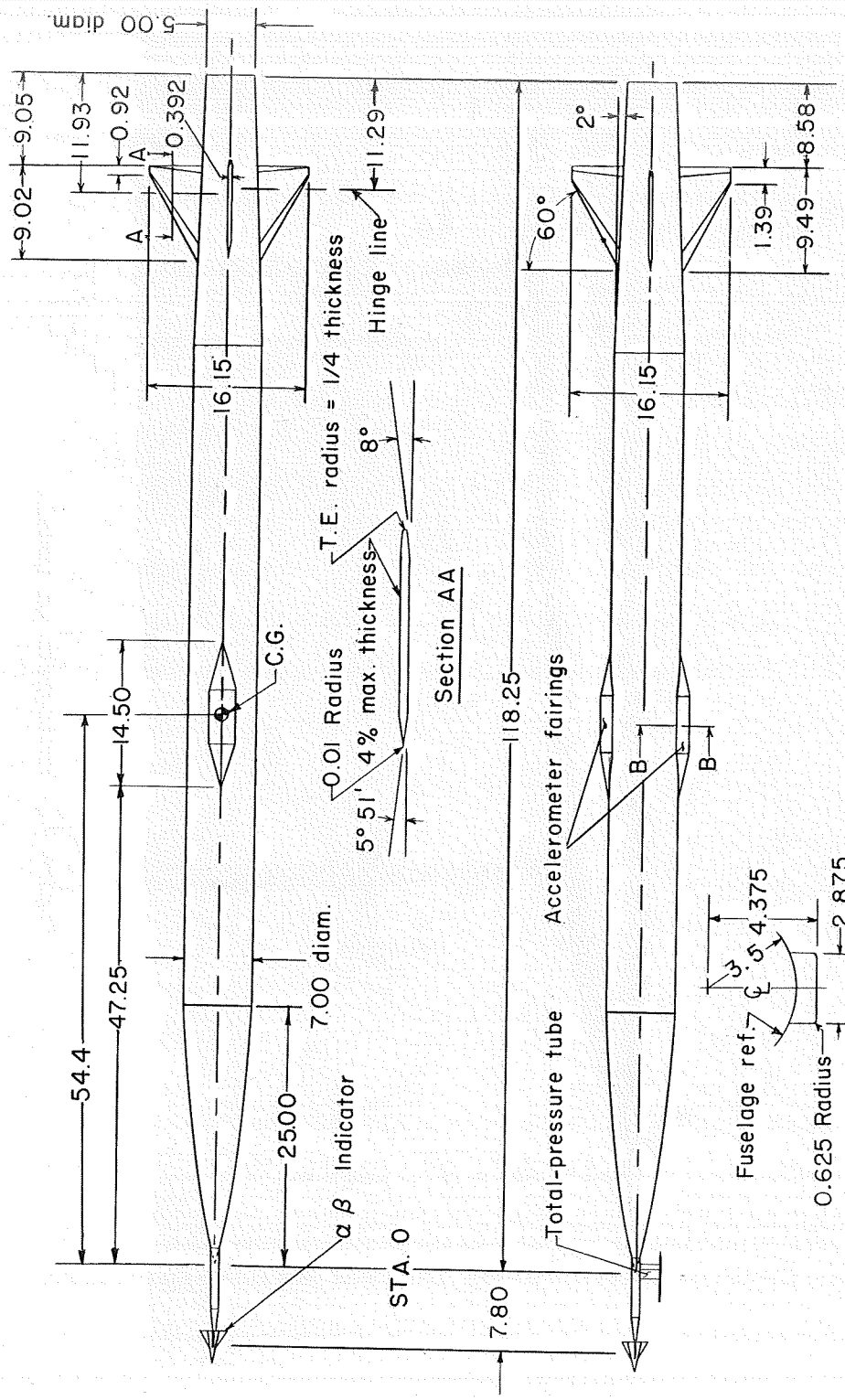

Figure 2.- Test configuration. All dimensions are in inches.

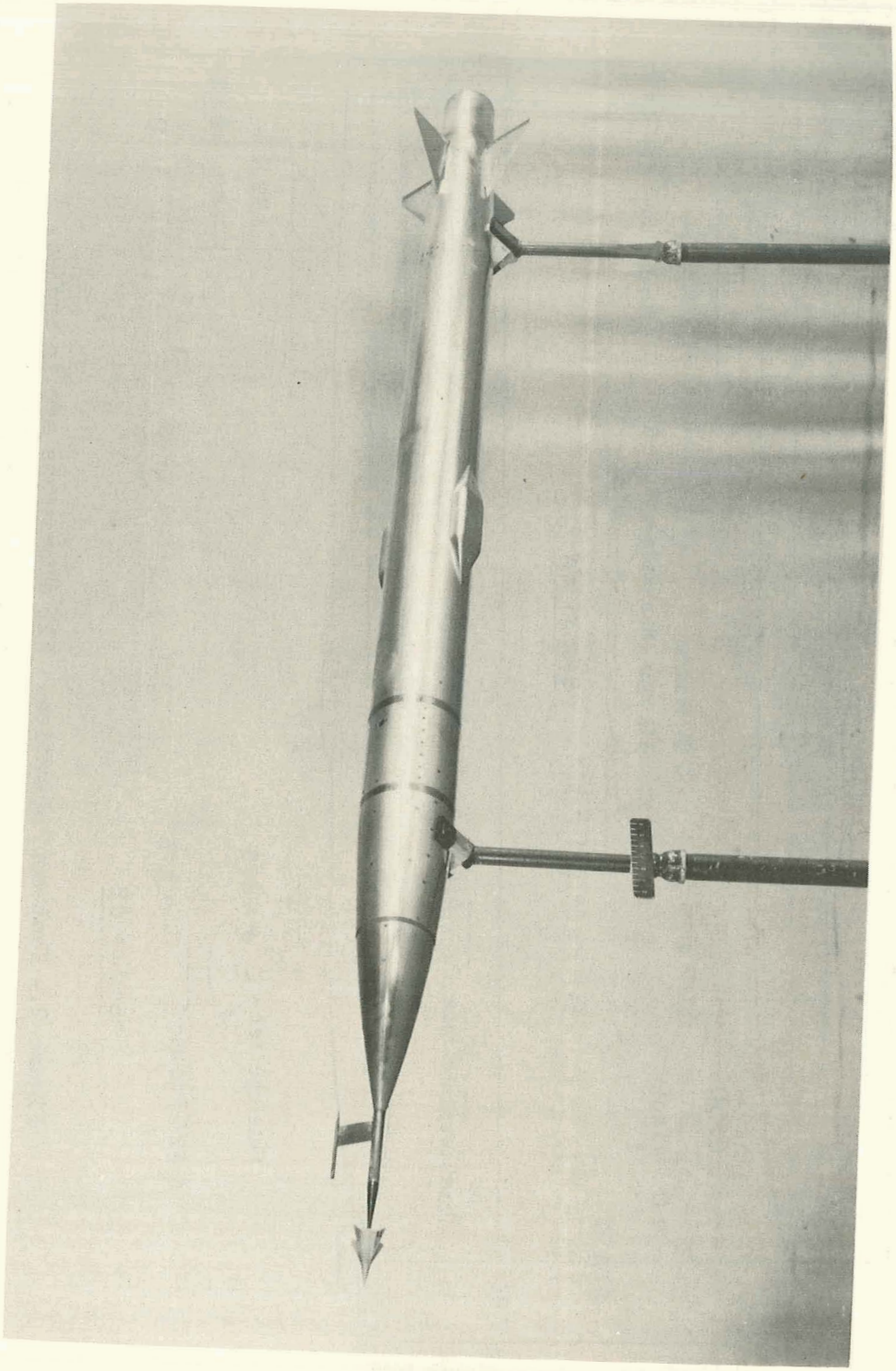

L-87338.1

Figure 3.- Photograph of model.

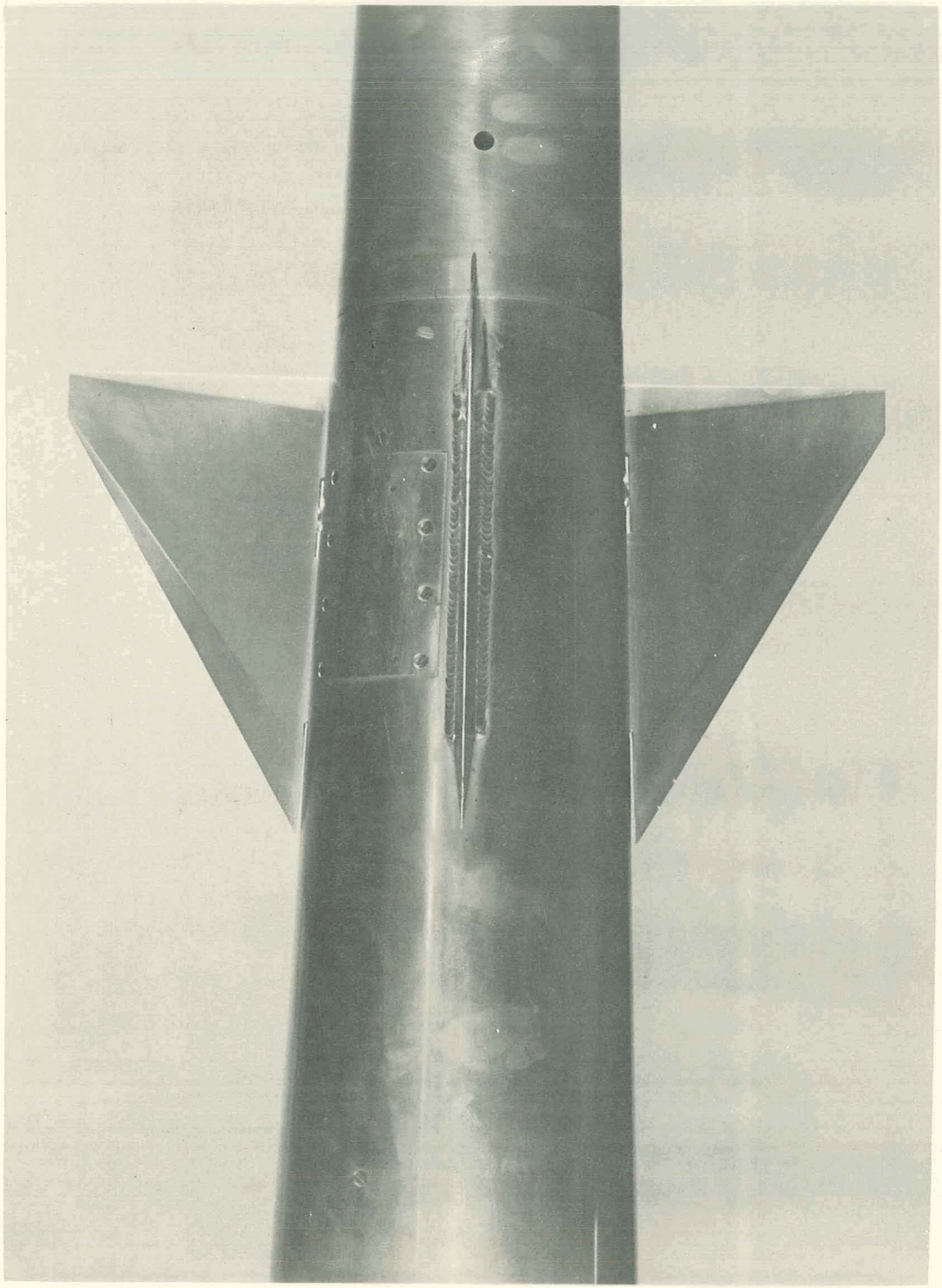

L-87339

Figure 4.- Photograph of hinged tail fins.

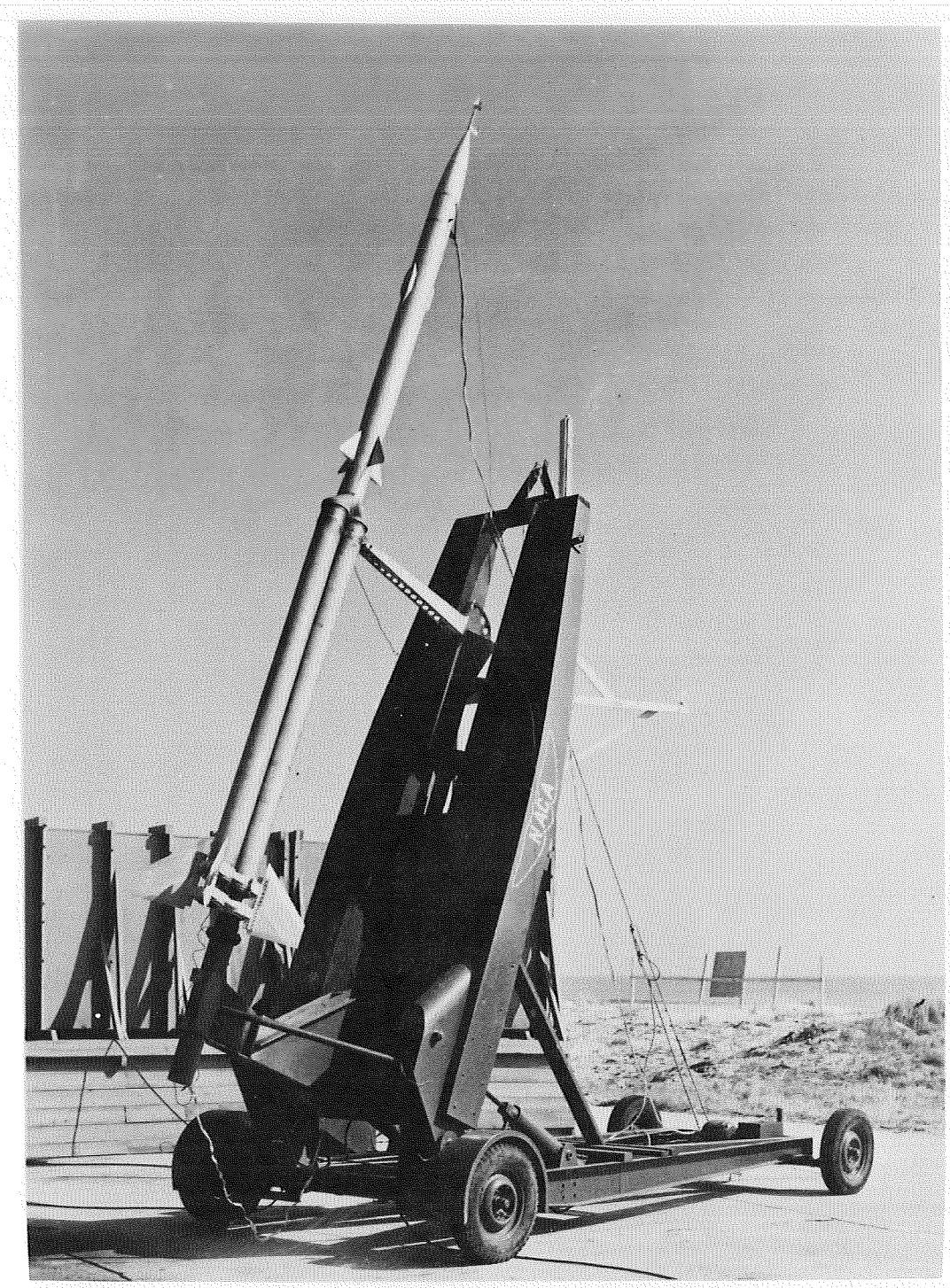

L-88358.1

Figure 5.- Model-booster combination.

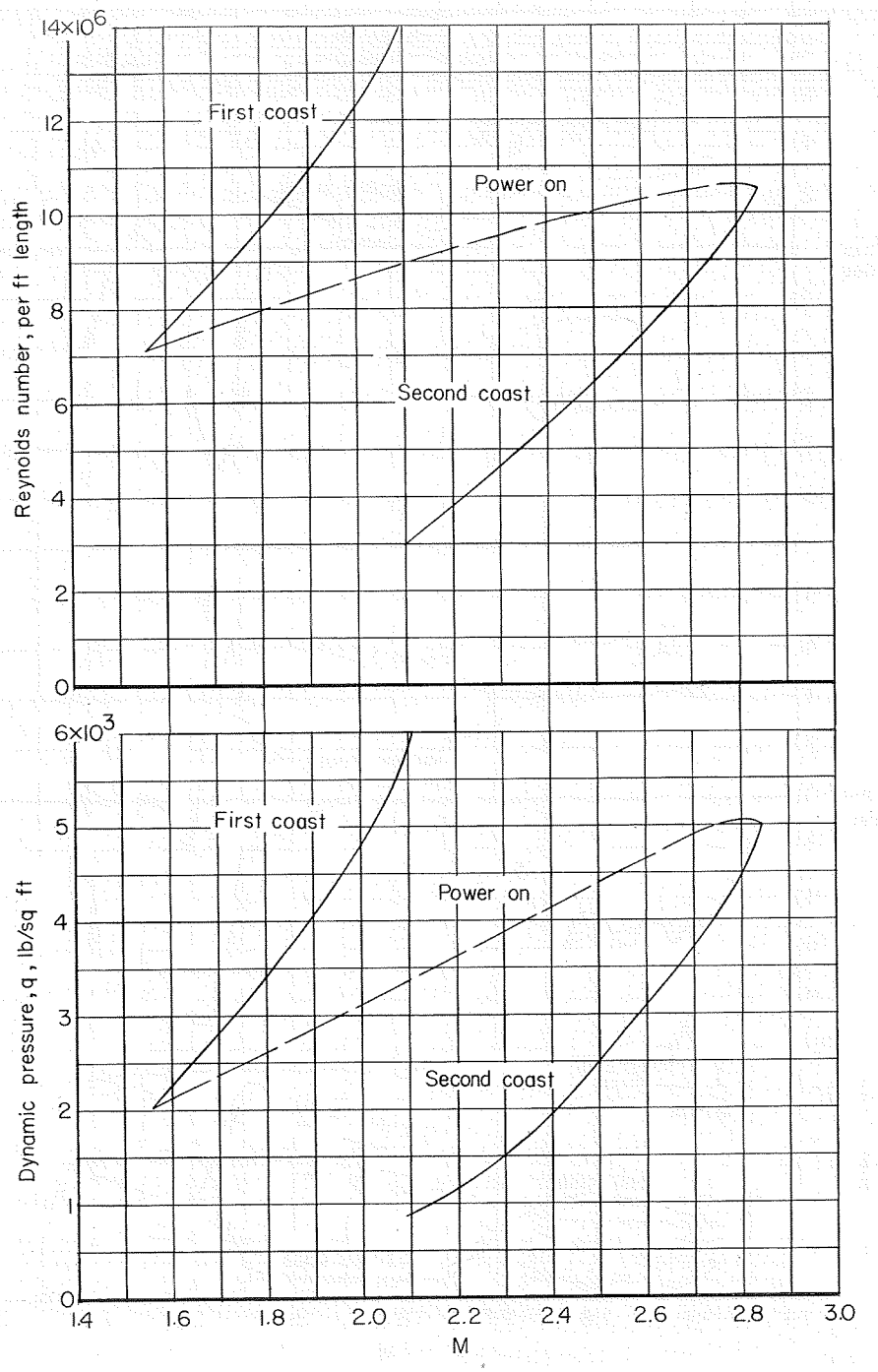

(a) Reynolds number and dynamic pressure.

Figure 6.- Flight-test conditions.

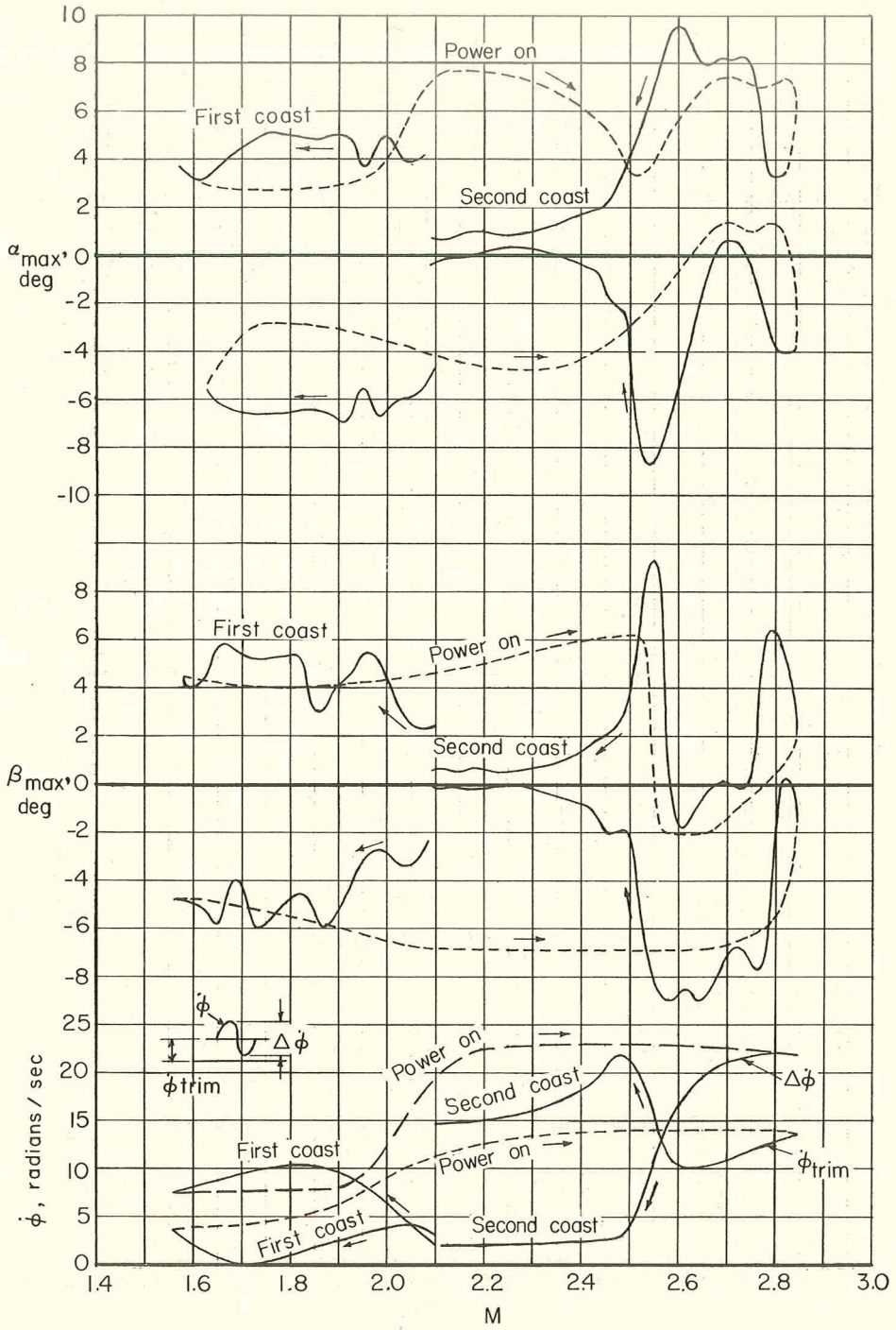

(b) Range of angle of attack, sideslip, and roll rate.

Figure 6.- Concluded.

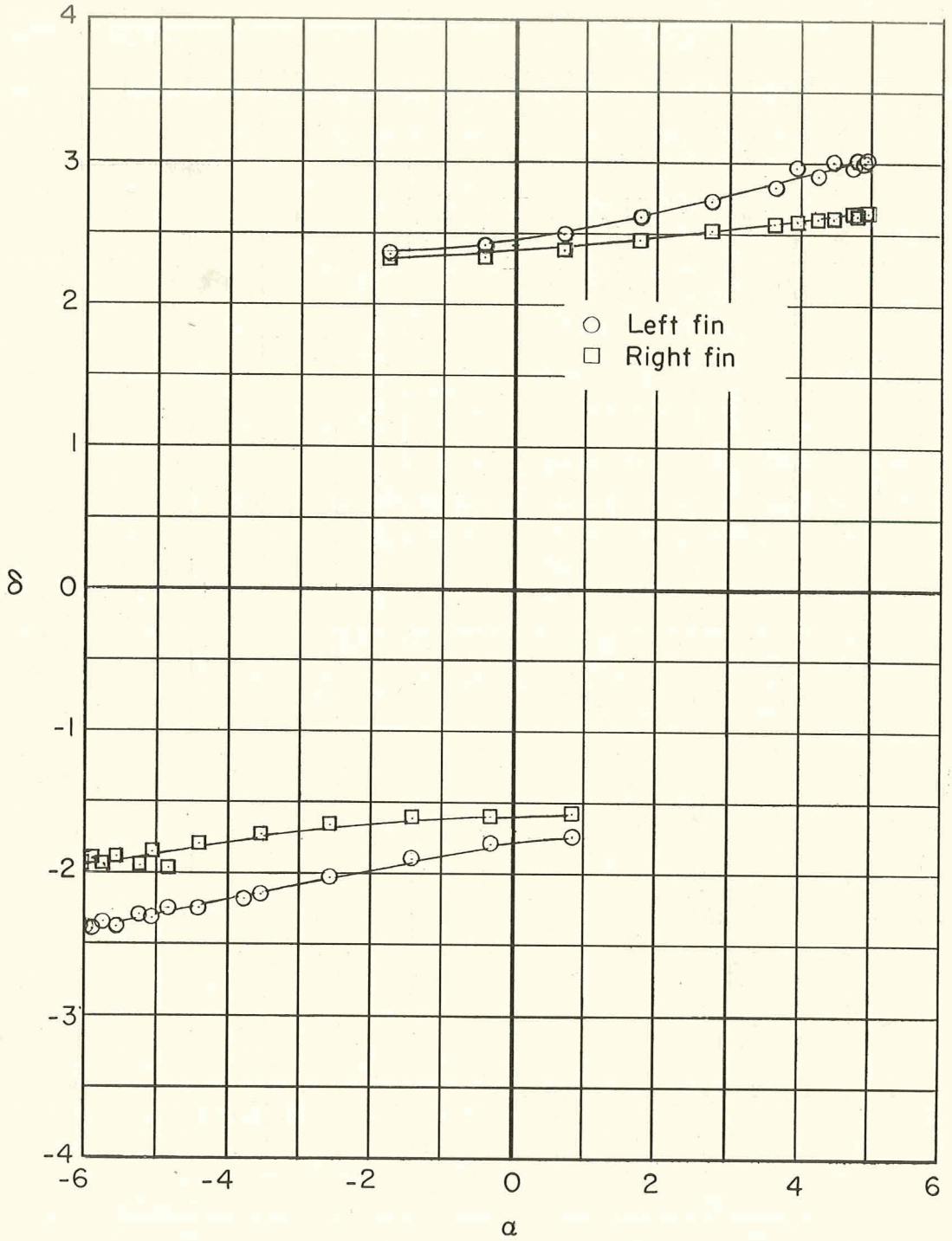

Figure 7.- Typical variation of tail setting with angle of attack. Mach number, 2.01; first coast period.

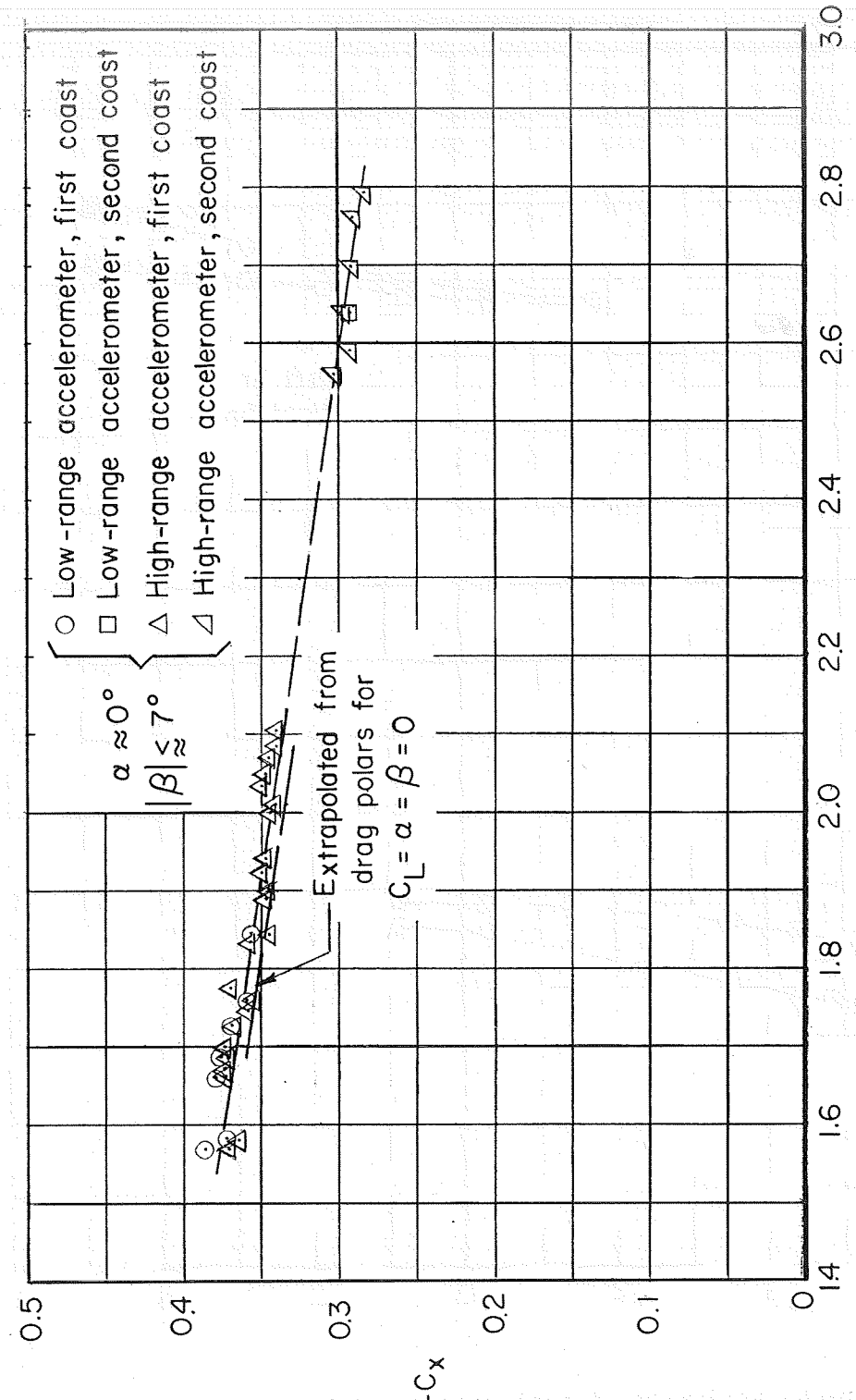

Figure 8.- Axial-drag coefficient based on maximum circular cross-sectional area of body.

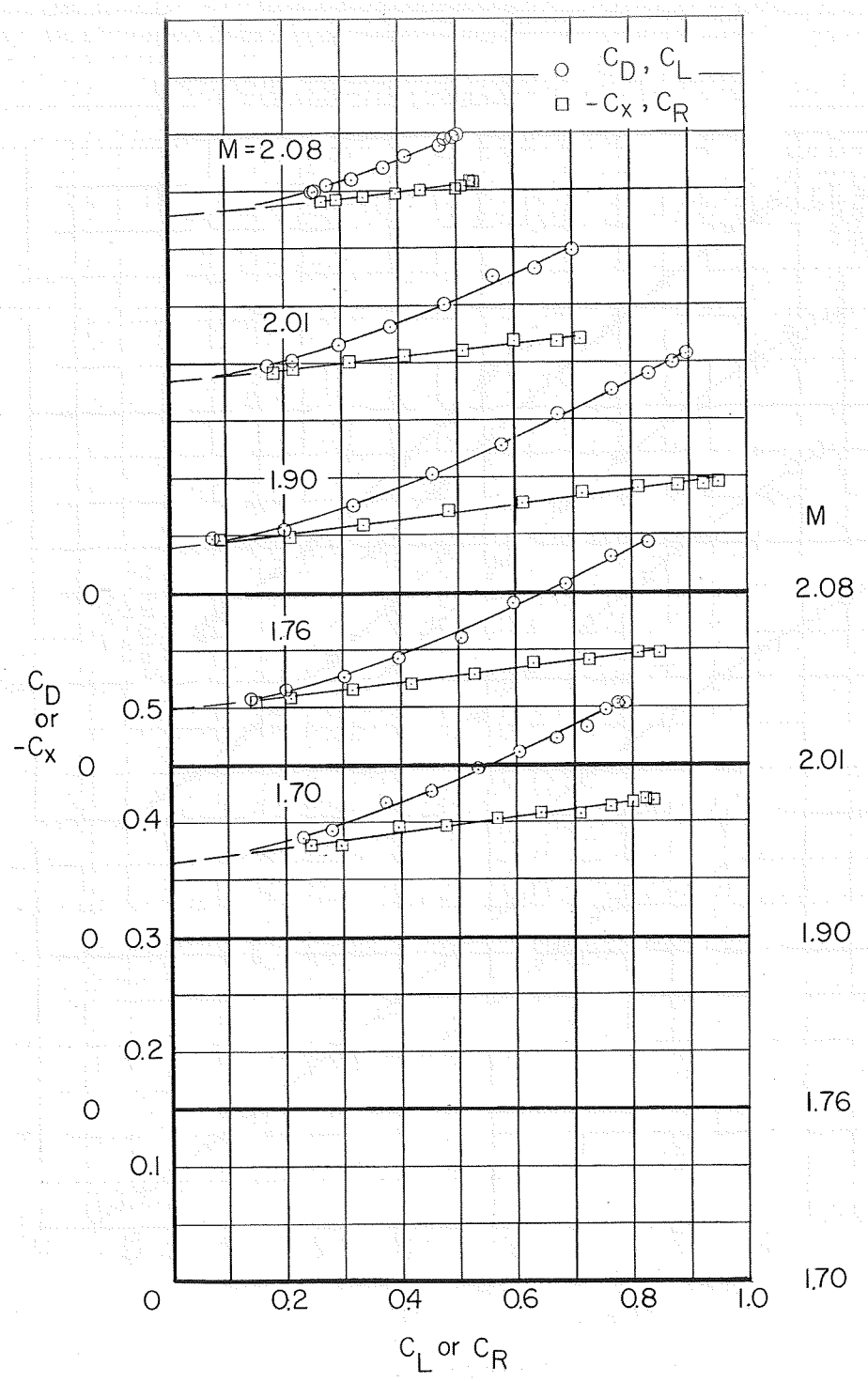

Figure 9.- Drag at lift, based on maximum circular cross-sectional area of body. First coast period.

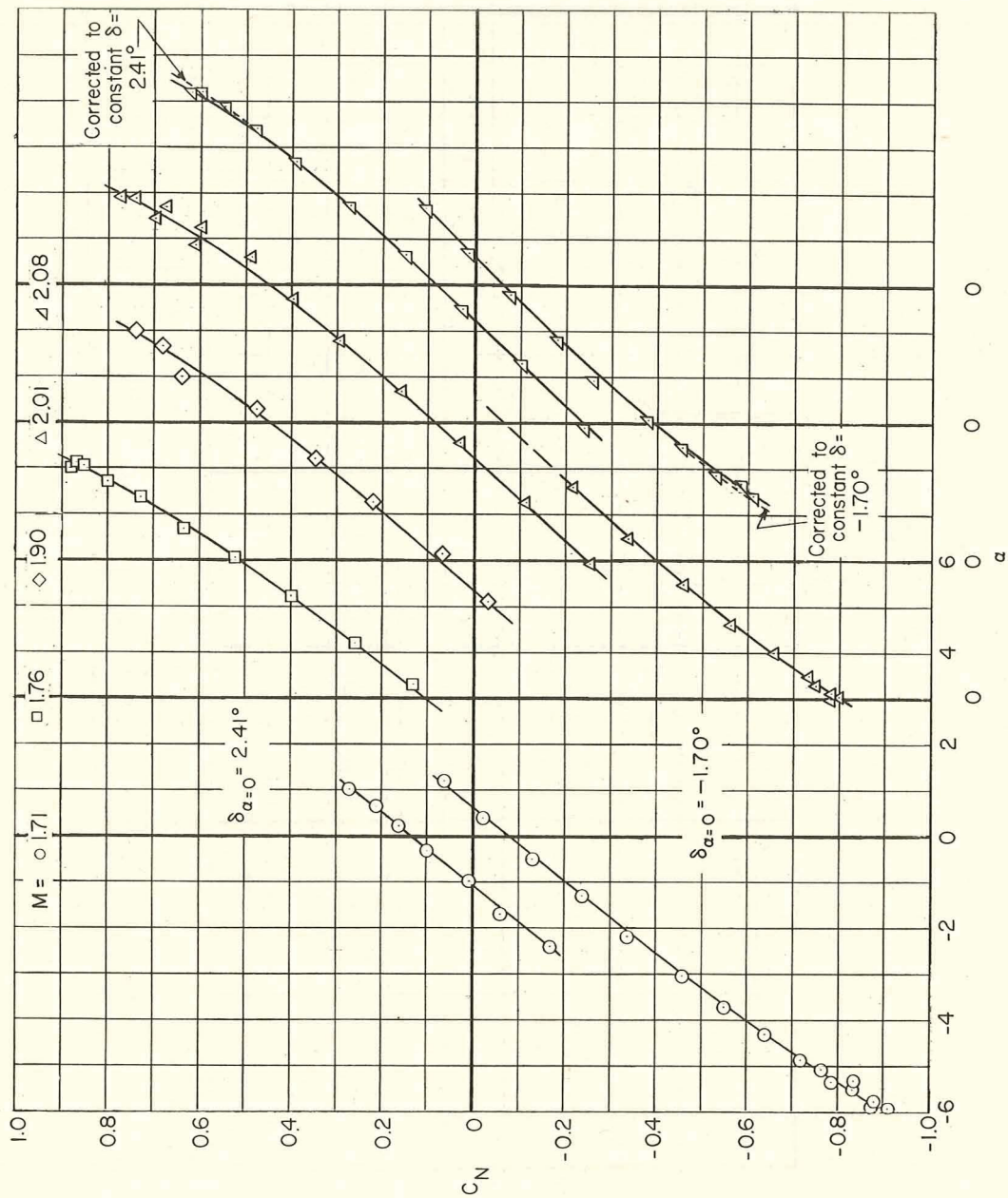

Figure 10.- Normal-force coefficient based on maximum circular cross-sectional area of body.

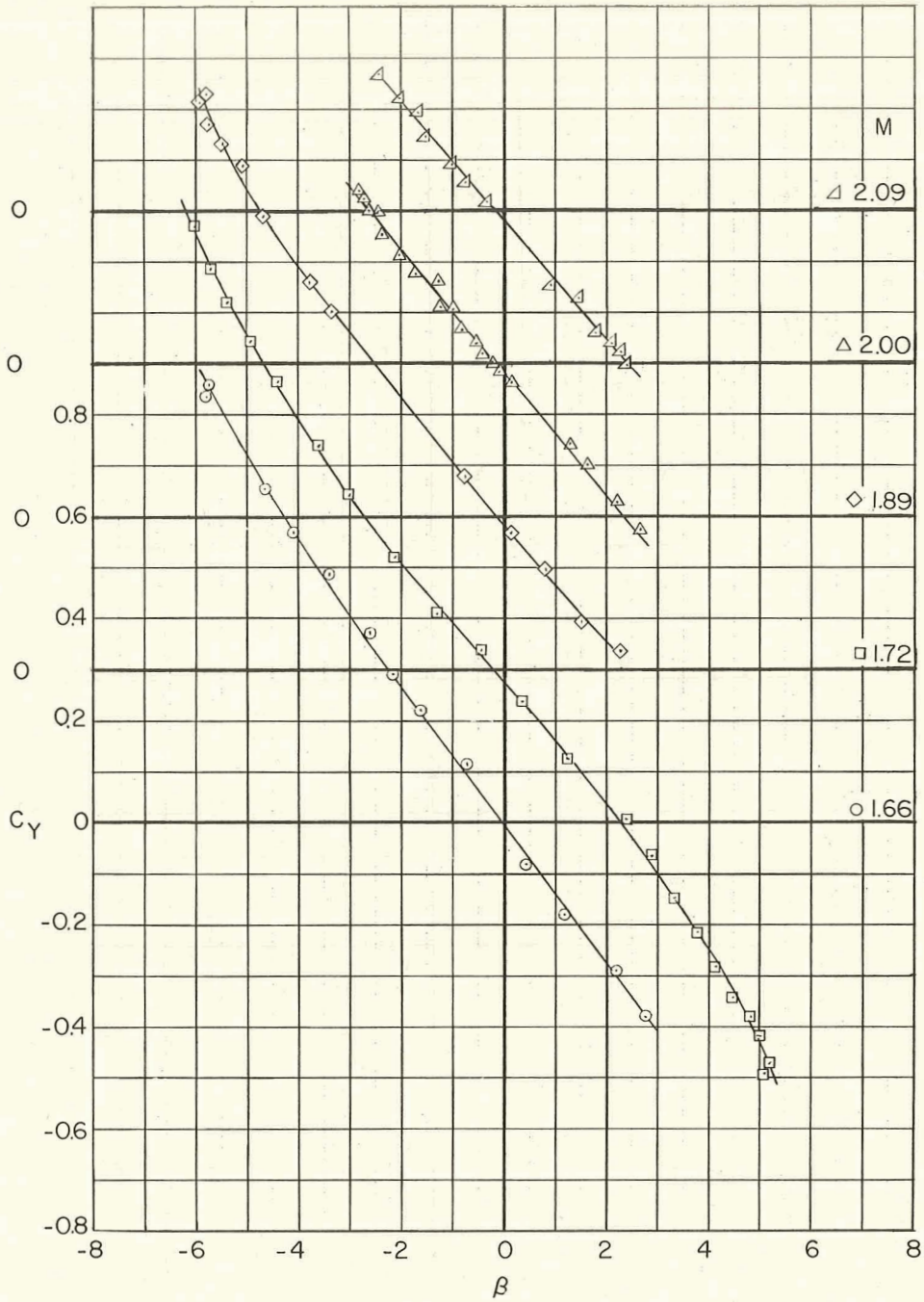

(a) First coast period.

Figure 11.- Side-force coefficient based on maximum circular cross-sectional area of body.

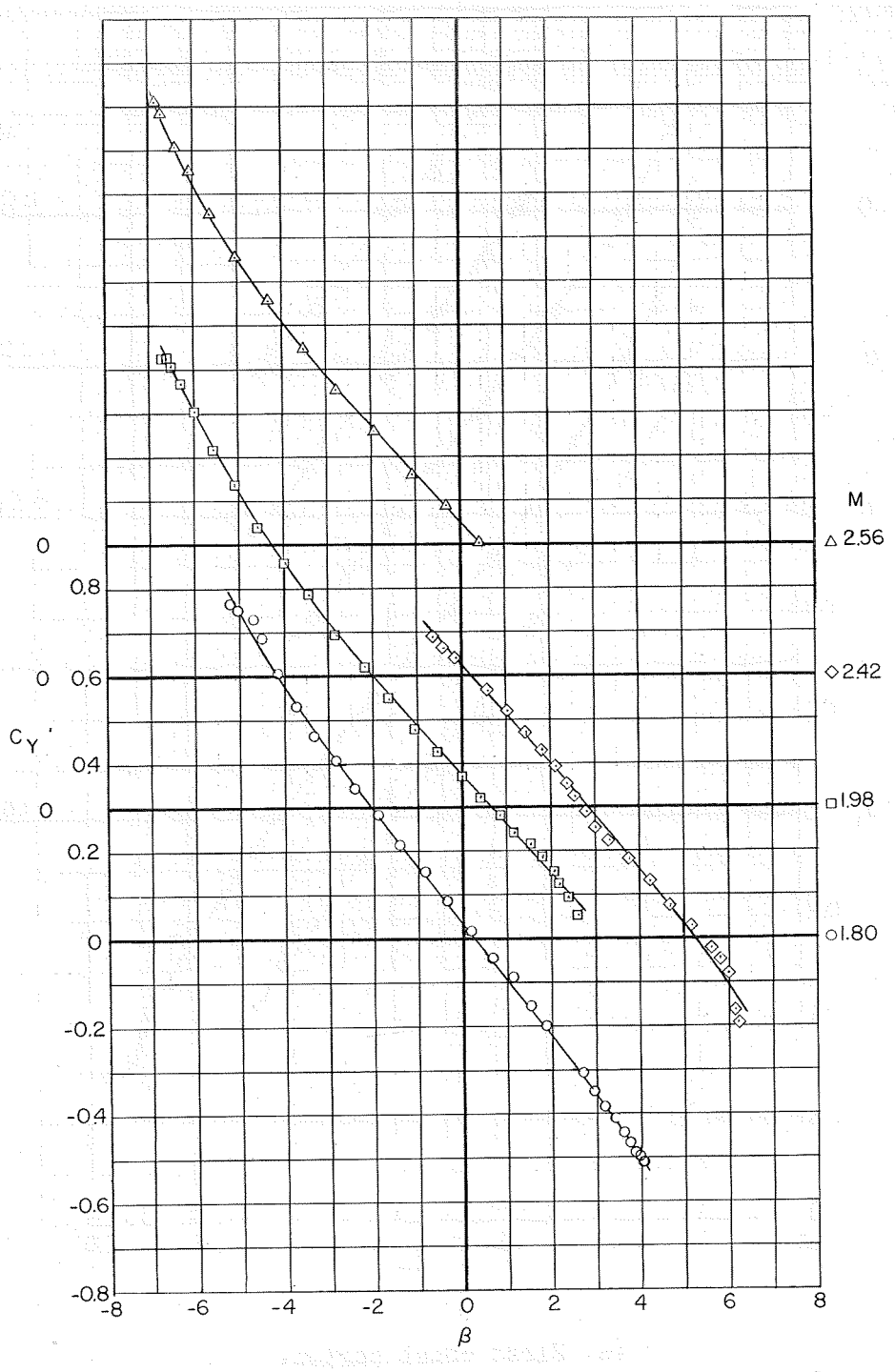

(b) Power-on period.

Figure 11.- Continued.

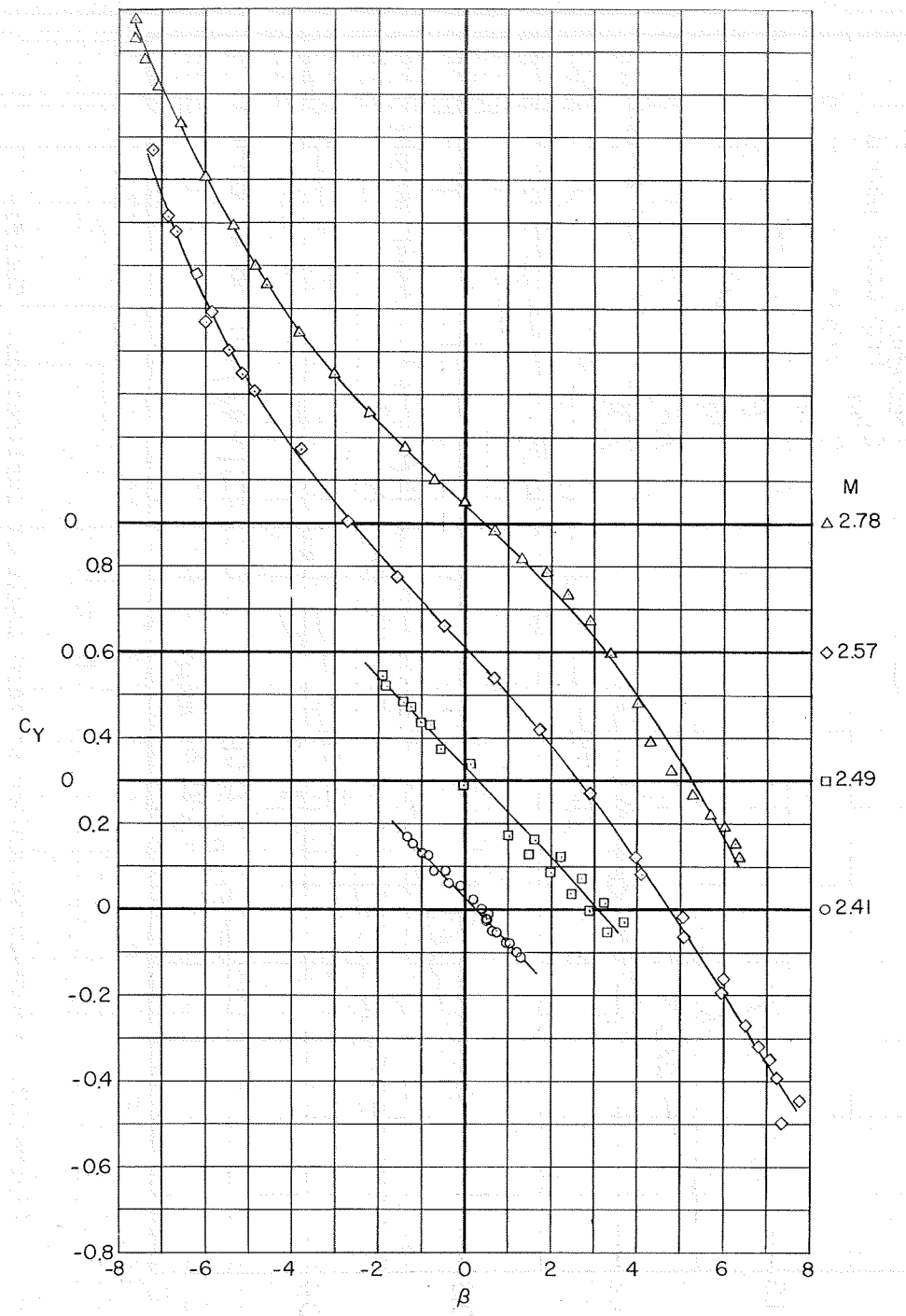

(c) Second coast period.

Figure 11.- Concluded.

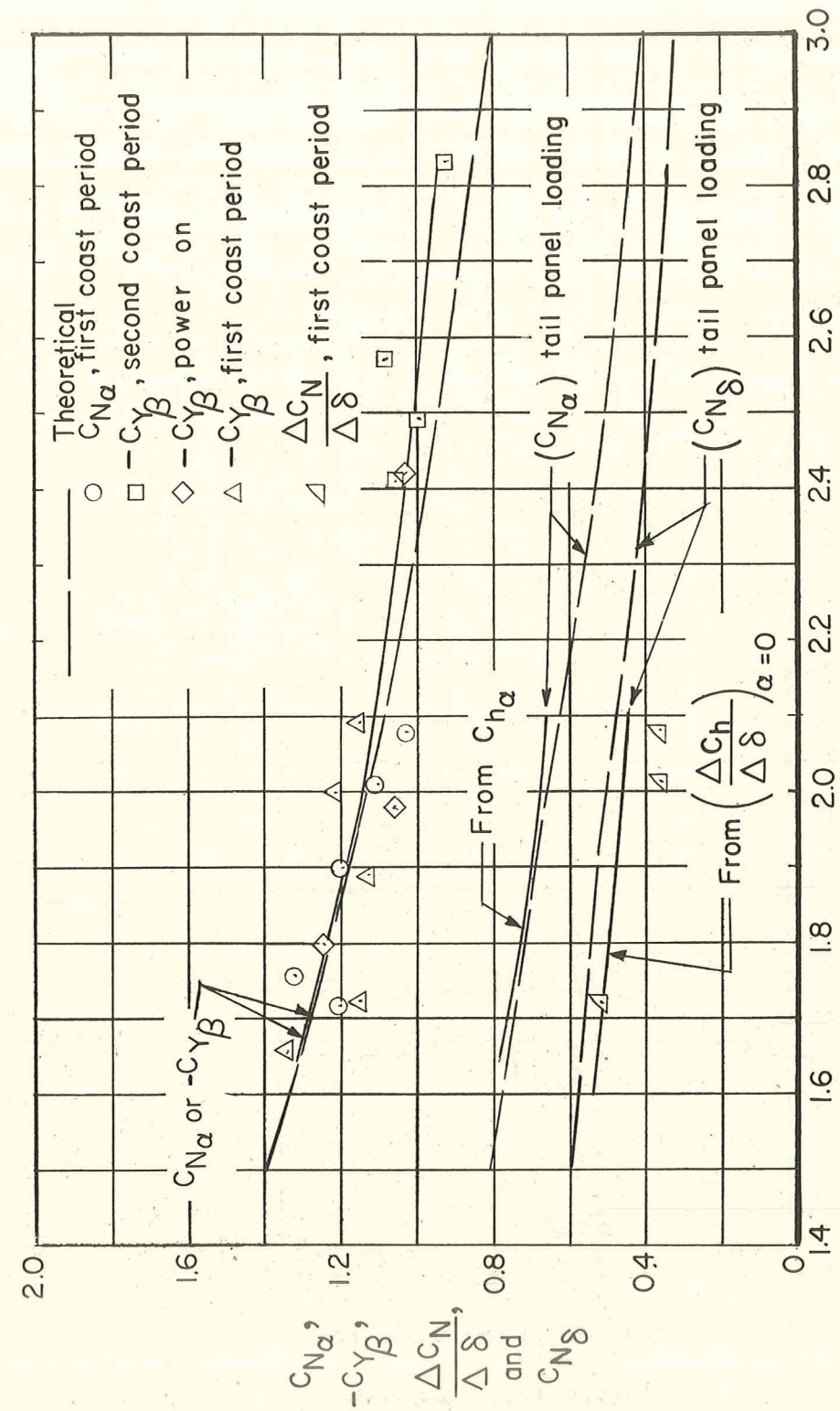

Figure 12.- Force-curve slopes at zero angle of inclination. Coefficients based on maximum circular cross-sectional area of body.

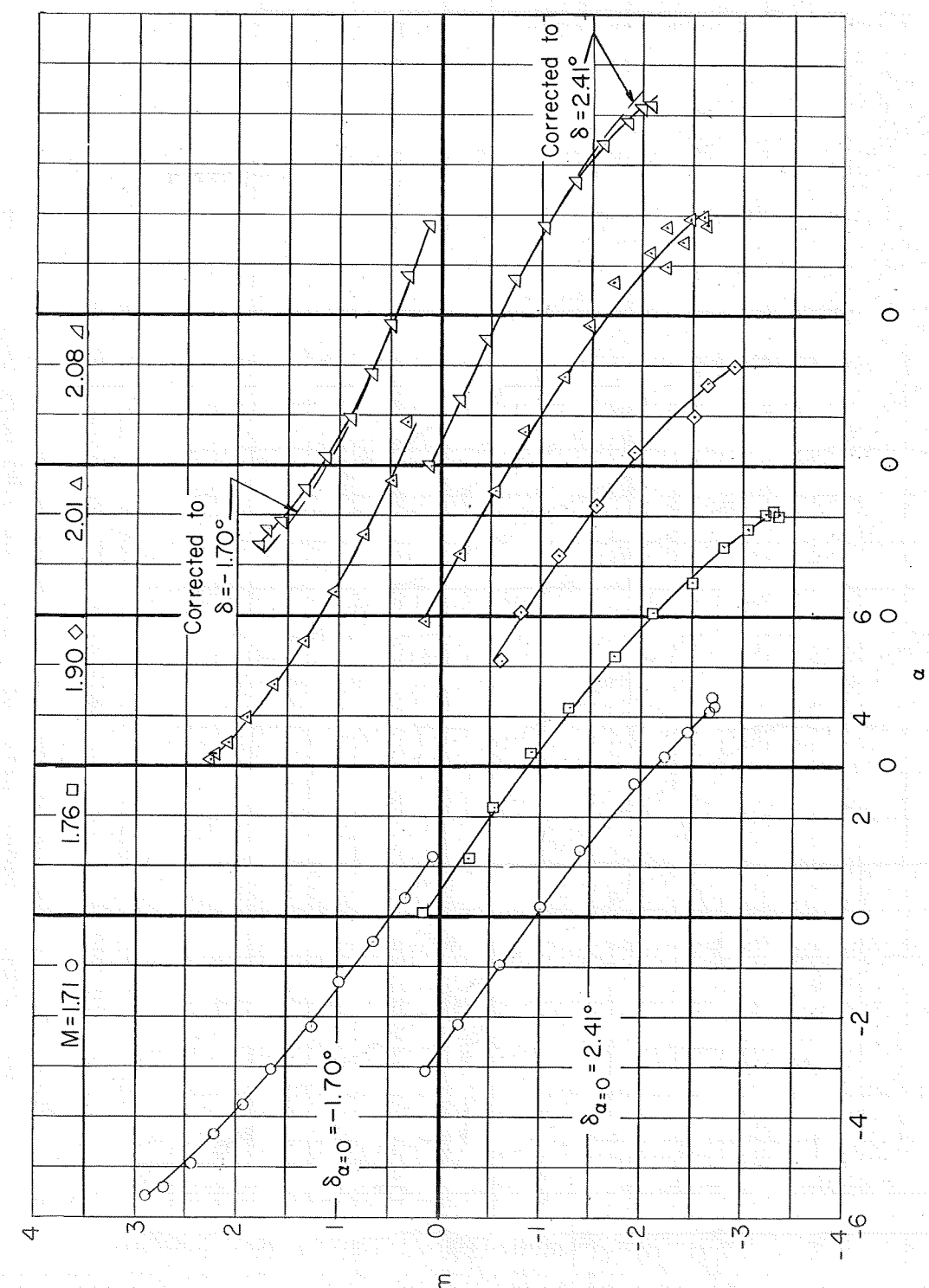

Figure 13.- Pitching-moment coefficient based on maximum circular cross-sectional area and diameter of body. First coast period.

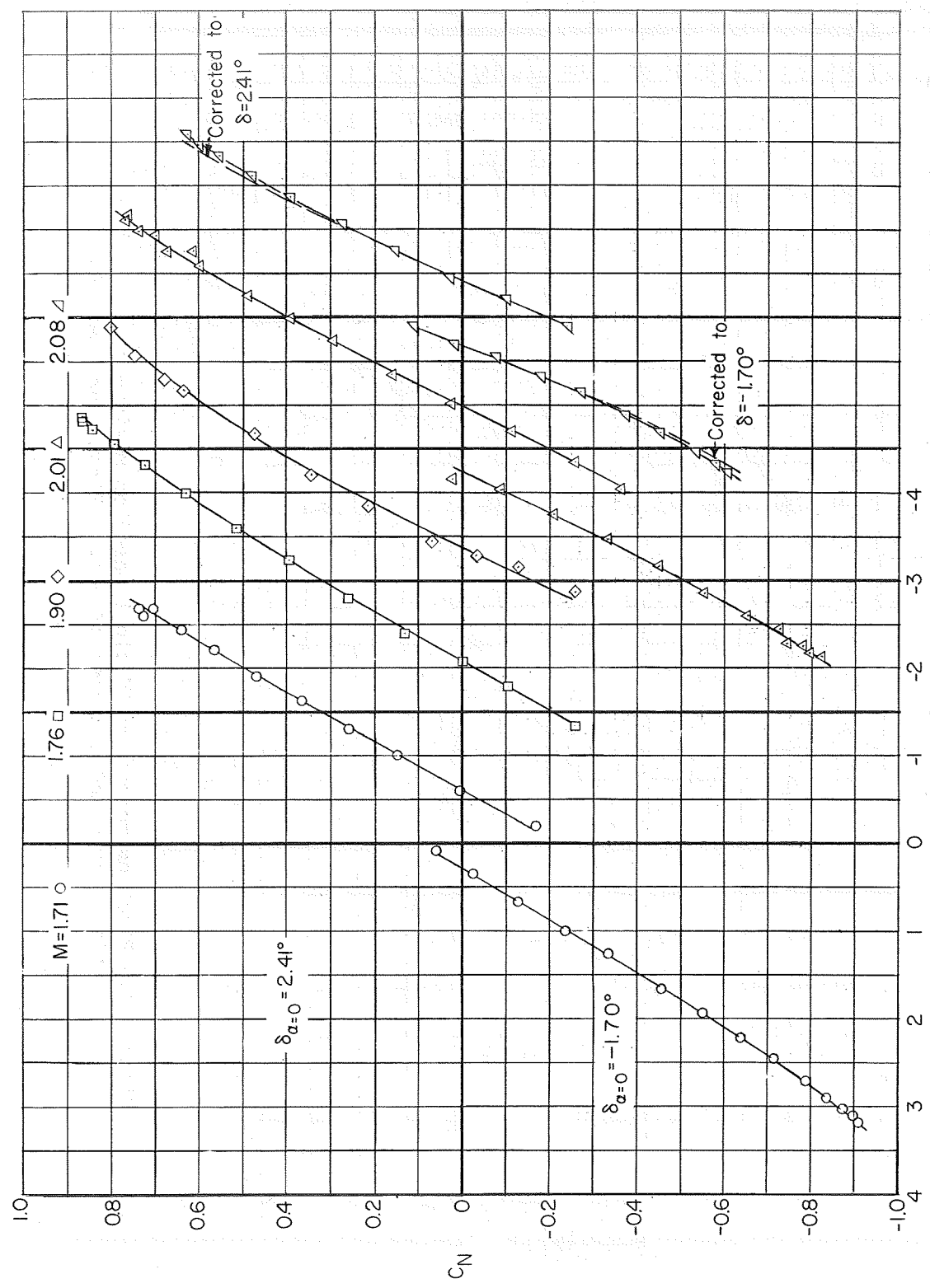

Figure 14.- Variation of normal-force coefficient with pitching-moment coefficient. Model center of gravity at 0.46 body length. Coefficients based on maximum circular cross-sectional area of body.

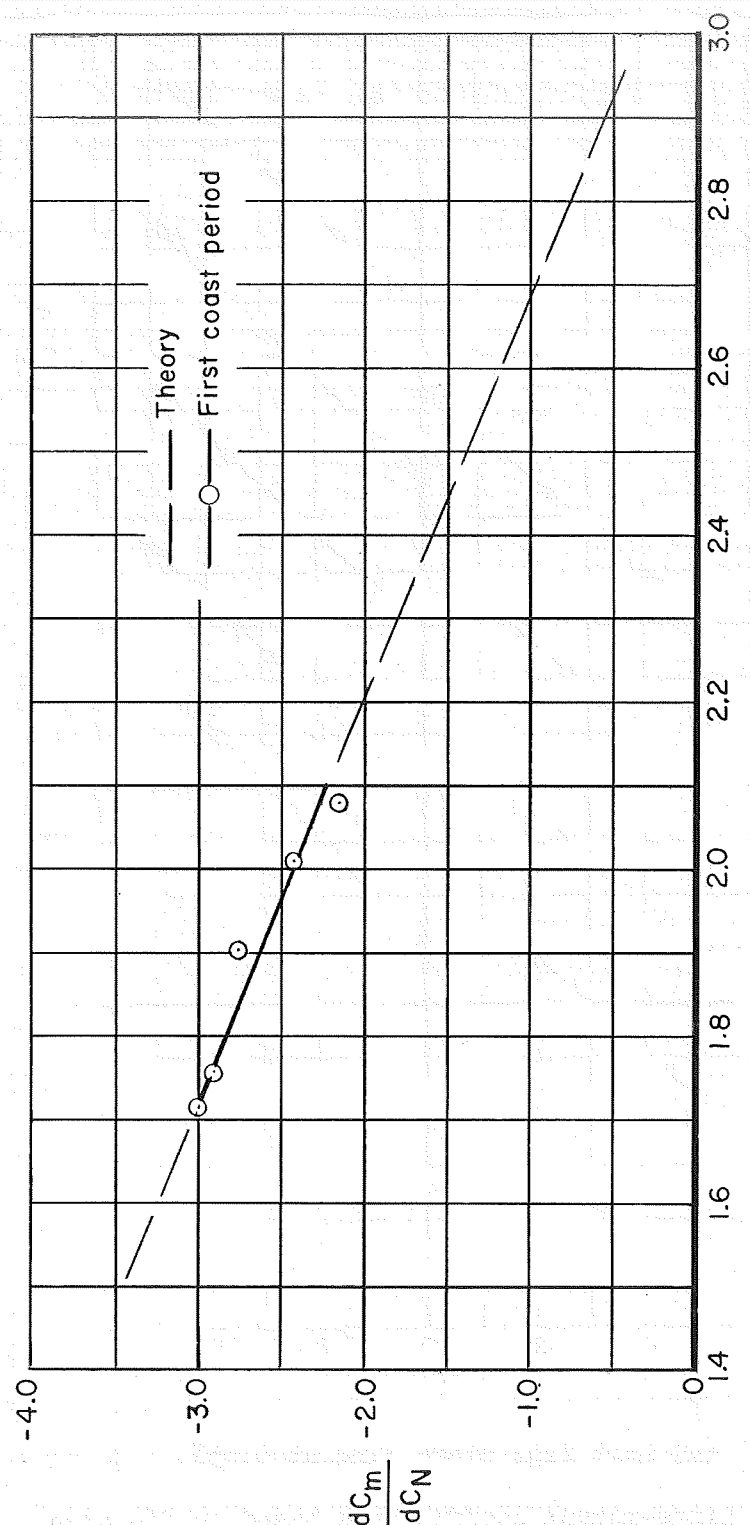

Figure 15.- Static-stability parameter dC_m/dC_N at zero angle of attack. Model center of gravity at 0.46 body length.

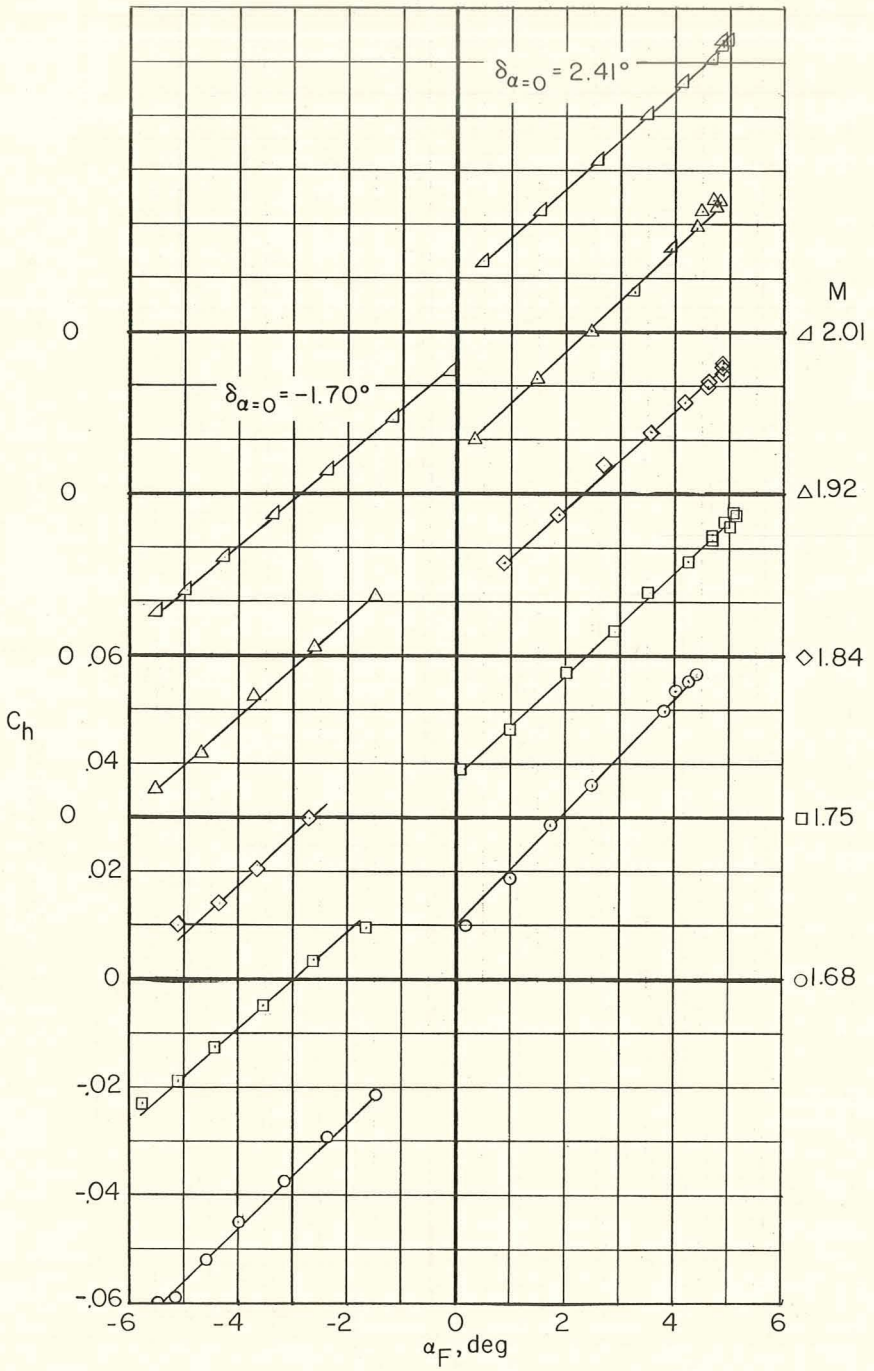

(a) Left fin; hinge line at $0.65\bar{c}$.

Figure 16.- Fin hinge-moment coefficients based on fin area. First coast period.

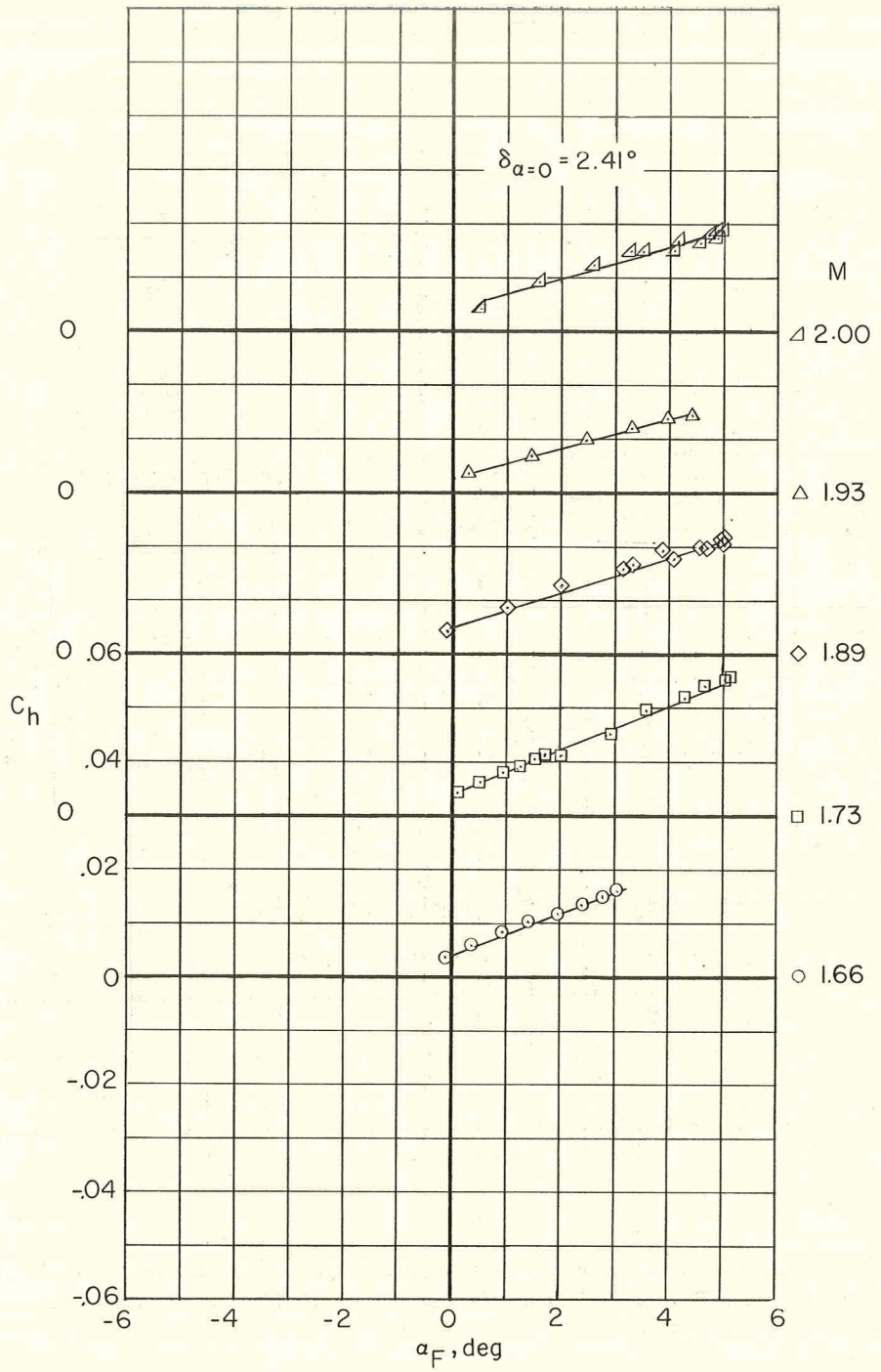

(b) Right fin; hinge line at $0.55\bar{c}$.

Figure 16.- Concluded.

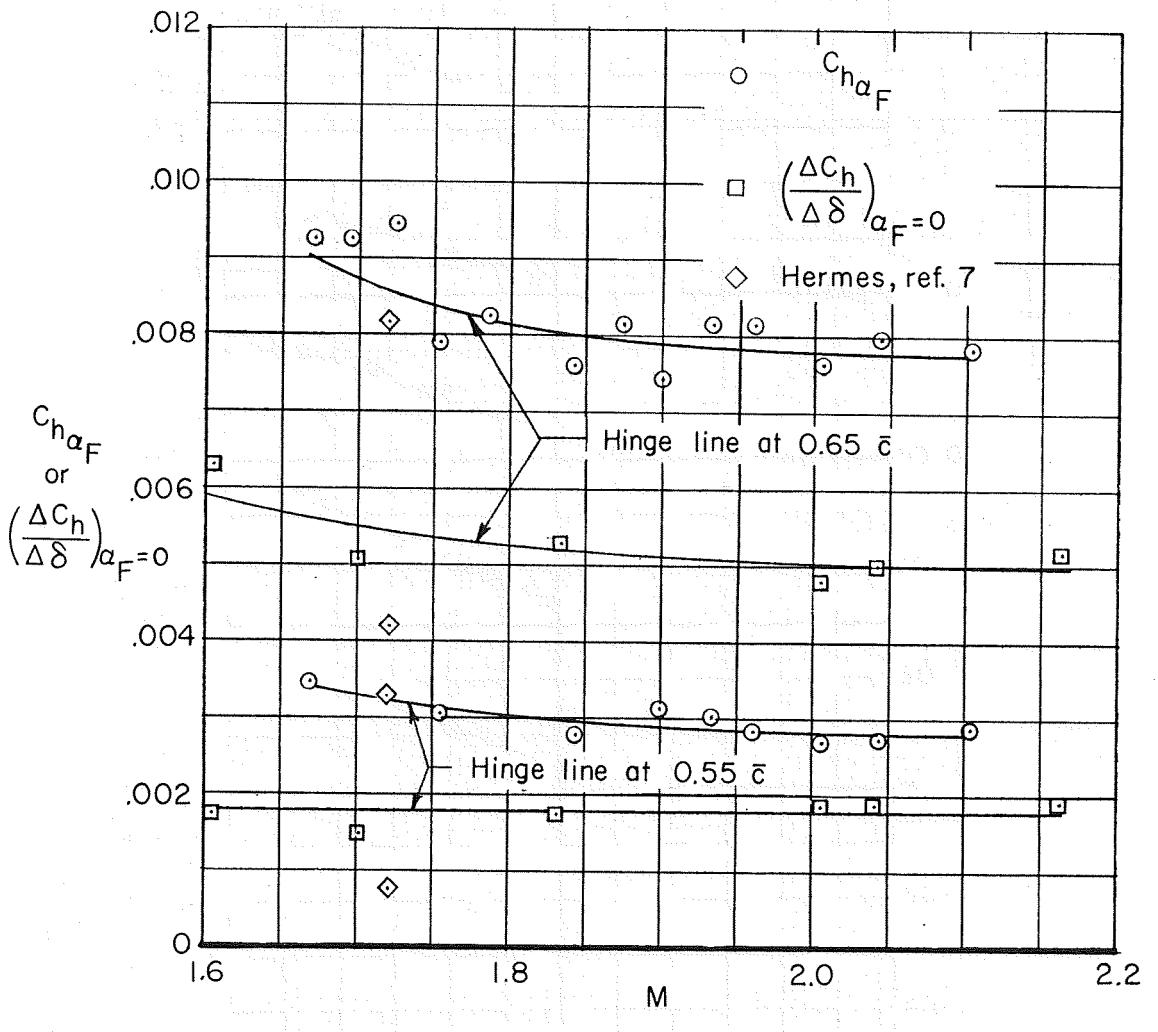

Figure 17.- Hinge-moment-coefficient slope due to angle of attack and incremental hinge-moment coefficient per unit fin deflection. Coefficients based on fin area.

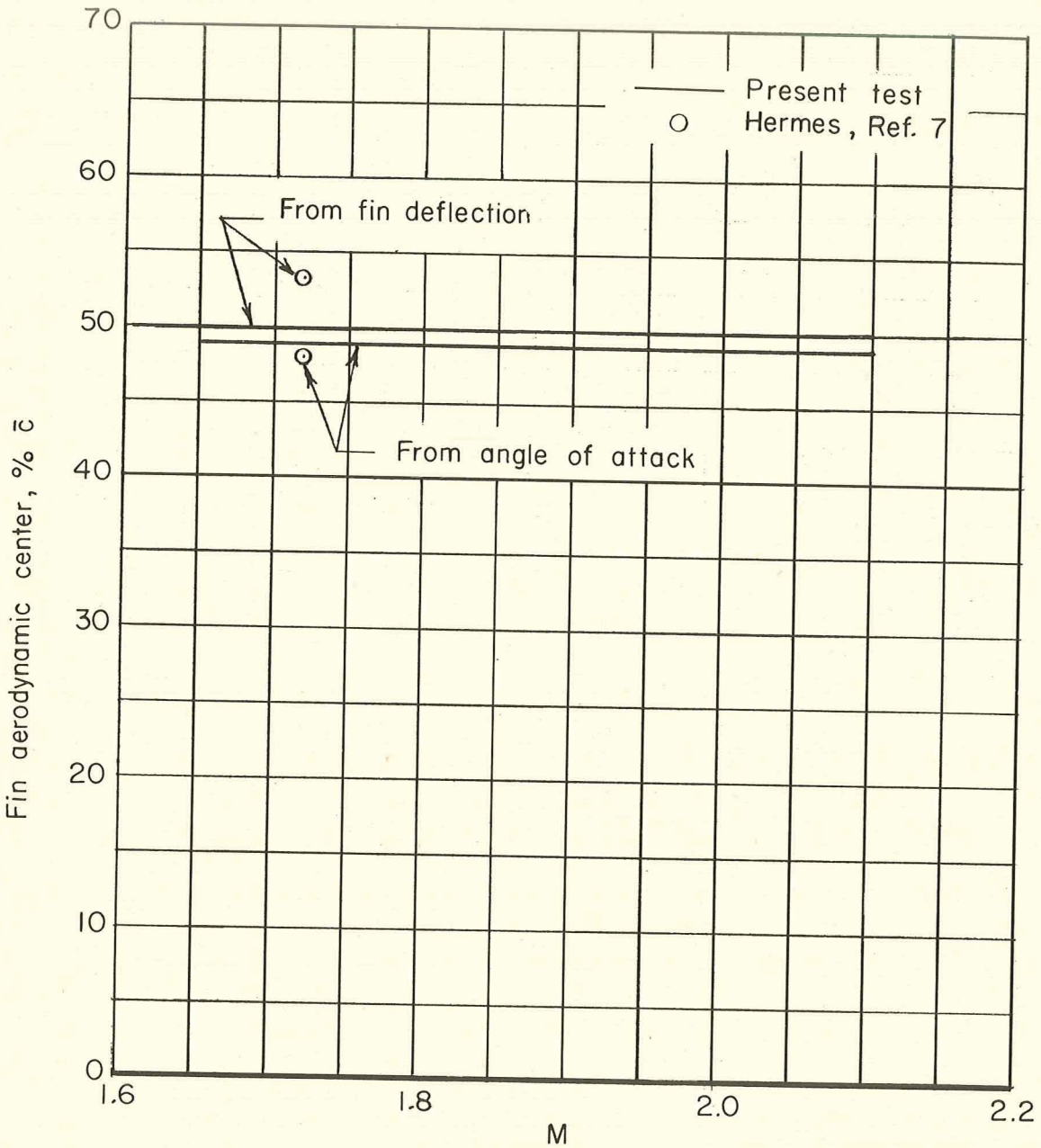

Figure 18.- Aerodynamic center of fin panel.